LANGMUIR Article
Cite This: Langmuir 2019, 35, 1902−1908
pubs.acs.org/Langmuir

# Spreading of Cell Aggregates on Zwitterion-Modified Chitosan Films

Baowen Qi,[†,‡,§] Haike Feng,[∥] Xingping Qiu,[‡] Grégory Beaune,[§] Xiaoqiang Guo,[†] Françoise Brochard-Wyart,[⊥] and Françoise M. Winnik*[,‡,§,&]

[†]College of Pharmacy and Biological Engineering, Chengdu University, Chengdu 610106, China
[‡]Département de Chimie, Université de Montréal, CP 6128 Succursale CentreVille, Montréal, QC H3C 3J7, Canada
[§]International Center for Materials Nanoarchitectonics (MANA), National Institute for Materials Science (NIMS), 1-1 Namiki, Tsukuba, Ibaraki 305-0044, Japan
[∥]College of Material, Chemistry and Chemical Engineering, Hangzhou Normal University, Hangzhou 310036, China
[⊥]Sorbonne Université, UMR 168, Institut Curie, 26 rue d'Ulm, 75248 Paris Cedex 05, France
[&]Laboratory of Polymer Chemistry, Department of Chemistry, University of Helsinki, P.O. Box 55, FI-00014 Helsinki, Finland

Supporting Information

**ABSTRACT:** The sulfobetaine (SB) moiety, which comprises a quaternary ammonium group linked to a negatively charged sulfonate ester, is known to impart nonfouling properties to interfaces coated with polysulfobetaines or grafted with SB-polymeric brushes. Increasingly, evidence emerges that the SB group is, overall, a better antifouling group than the phosphorylcholine (PC) moiety extensively used in the past. We report here the synthesis of a series of SB-modified chitosans (CH-SB) carrying between 20 and 40 mol % SB per monosaccharide unit. Chitosan (CH) itself is a naturally derived copolymer of glucosamine and *N*-acetyl-glucosamine linked with a $\beta$-1,4 bond. Analysis by quartz crystal microbalance with dissipation (QCM-D) indicates that CH-SB films (thickness ∼ 20 nm) resist adsorption of bovine serum albumin (BSA) with increasing efficiency as the SB content of the polymer augments (surface coverage ∼ 15 $\mu$g cm$^{-2}$ for films of CH with 40 mol % SB). The cell adhesivity of CH-SB films coated on glass was assessed by determining the spreading dynamics of CT26 cell aggregates. When placed on chitosan films, known to be cell-adhesive, the CT26 cell aggregates spread by forming a cell monolayer around them. The spreading of CT26 cell aggregates on zwitterion-modified chitosans films is thwarted remarkably. In the cases of CH-SB30 and CH-SB40 films, only a few isolated cells escape from the aggregates. The extent of aggregate spreading, quantified based on the theory of liquid wetting, provides a simple *in vitro* assay of the nonfouling properties of substrates toward specific cell lines. This assay can be adopted to test and compare the fouling characteristics of substrates very different from the chemical viewpoint.

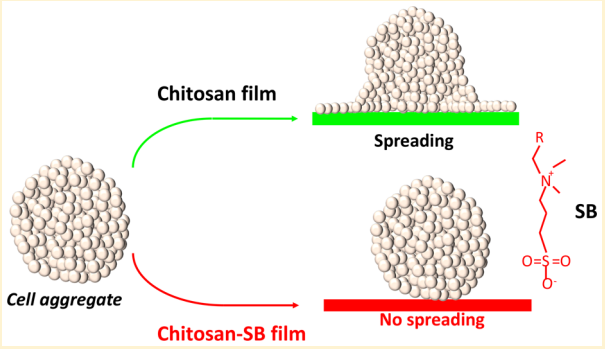


## INTRODUCTION

Innovations in the synthesis and fabrication of biomaterials have enabled major advances in tissue engineering, treatment of cardiovascular diseases, cancer therapy, and development of long-lasting surgical implants. The cellular response to a polymeric substrate is affected by numerous factors, such as surface chemistry, topography, rigidity, wettability, and surface charge.[1] Conversely, specific demands are placed on biomaterials depending on their intended use. Some applications require platforms promoting cell adhesion,[2] directed cell migration,[3] or cell differentiation.[4] In contrast, in the context of cardiovascular implants, materials must resist cell adhesion to prevent stenosis.[5,6] Poly(ethylene glycols)[7] and zwitterionic polymers[8] are among the most successful nonfouling coatings currently available. The outstanding nonfouling characteristics of polyzwitterions are attributed to their high degree of hydration[8−10] and the preferred orientation of the bound water molecules.[11,12] Among zwitterionic moieties, phosphorylcholine (PC), sulfobetaines (SB), and carboxybetaines (CB) are used most commonly. The PC group comprises of a positively charged trimethylammonium group and a negatively charged phosphate ester.[13] In the SB and CB groups the anionic moieties are sulfonate esters and carbonate esters, respectively.[14,15] While all three families act as nonfouling agents, they show subtle differences in properties such as stability and resistance against oxidation.[16]

Special Issue: Zwitterionic Interfaces: Concepts and Emerging Applications

Received: July 20, 2018
Revised: August 16, 2018
Published: August 24, 2018

Several years ago, we coupled phosphorylcholine groups to the amine moieties of chitosan, a biocompatible and bioadhesive copolymer of glucosamine and *N*-acetyl-glucosamine linked by a $\beta$-1,4 bond.[17] Our objective was to obtain chitosan derivatives soluble under physiological conditions in order to facilitate their use in biological media. The strategy was successful, chitosan with ∼40 mol % PC per mol of monosaccharide (CH-PC40) was soluble in water over the entire pH range. We also observed that protein adsorption was low on all CH-PC films immersed in aqueous protein solutions and that the protein surface density decreased markedly with increasing PC content of the substrate.[18] Both human umbilical vein endothelial cells (HUVEC) and a human breast cancer cell line (MCF-7) adhered poorly on CH-PC films. Cells showed a marked tendency to aggregate on the substrates,[21] a phenomenon typical for cohesive cells seeded on nonfouling substrates. In contrast, on fouling films cells spread as isolated entities over the entire area of the film. Although CH-PC derivatives possess the solubility in physiological media and biocompatibility necessary for therapeutic applications, their high cost limits their routine applications as biomaterials.

Aware of the excellent nonfouling characteristics of polysulfobetaines,[19] we synthesized SB-modified chitosans (CH-SB) of increasing SB content and assessed their fouling properties. The outcome of this study is presented here. To test the *in vitro* fouling properties of CH-SB substrates, we devised a new test based on the spreading of cell aggregates on surfaces. Cell aggregates consist of thousands of cells assembled into spheroids via interactions between cadherin receptors on the cell surface. The cohesion of cell aggregates, which depends on the level of cadherin expression on their surface, is determined by $W_{CC,}$ the cell/cell adhesion energy per unit area. The statics and dynamics of spreading of cell aggregates deposited on a surface were analyzed in the framework of wetting by Steinberg in the early 1960s and by Brochard-Wyart and co-workers over the last decades.[20−22] The regimes of wetting are characterized by a spreading parameter, $S$, defined as $S = W_{CS} - W_{CC}$, where $W_{CS}$ is the cell/substrate adhesion energy per unit area. If the cell/cell adhesion energy is higher than the cell/substrate adhesion energy ($S < 0$, partial wetting), the aggregate at equilibrium forms a spherical cup with a finite contact angle (partial wetting). If $S > 0$ the aggregate spreads on the substrate by expanding outward a cell monolayer (complete wetting). The spreading dynamics of this precursor film result from the balance of the friction forces associated with the entry of cells from the aggregate into the cell monolayer and the active forces driving the motile cells at the periphery of the film.[21,22]

Within the context of the study reported here, it was important to select a cell line sufficiently cohesive to form aggregates, yet able to spread on typical cell adhesive substrates. We chose the murin colon carcinoma CT26 cell line, which is readily available and used extensively *in vitro* to model cancer tumors.[23] We gauged the cell adhesivity of CH-SB films coated on glass substrates by determining the spreading dynamics of CT26 cell aggregates on a set of CH-SB films (20 < SB < 40 mol %) over a 24-h period. We performed the same tests on fibronectin, a standard cell-adhesive surface, CH, and CH-PC20. The study provides guidelines for the design, synthesis, and evaluation of chitosan-based substrates ranging from cell-adhesive to nonfouling. This assay may prove valuable to test a much broader spectrum of substrates, as it is simple and the equipment necessary to perform it is available in most cell biology laboratories.

## EXPERIMENTAL SECTION

**Materials.** Chitosan (degree of deacetylation, DDA ∼ 75%), fibronectin, magnesium nitrate, sodium hydroxide, sodium acetate, 3-dimethylaminopropane 1, 2-diol, sodium periodate, 1, 3-propanesultone, and acetic acid were purchased from Aldrich Chemical Co. Streptomycin and penicillin were purchased from Gibco BRL. Deacetylated chitosan (2 mol % *N*-acetylamine groups, DDA ∼ 98%)[17] and phosphorylcholine-chitosan (CH-PC20)[18] were prepared as reported previously. Spectra/Pore membranes (Spectrum) were employed for dialysis. All solvents were of reagent grade and used as received. Water was deionized using a Milli-Q water purification system (Millipore). $^1$H NMR spectra were recorded on a Bruker ARX-400 400 MHz spectrometer using $D_2O$/DCl 100/1 v/v) as the solvent. Mass spectra were recorded on a Micromass Autospec TOF instrument equipped with a LSIM source (Regional Center of Mass Spectrometry, University of Montreal, Montreal, QC, Canada). Quartz crystal microbalance with dissipation (QCM-D) experiments were carried out with a Q-sense model E4 instrument. Polished AT-cut 5 MHz quartz crystal sensors (Quartz Pro) with gold electrodes were used as substrates. Five QCM overtones (15, 25, ..., 55 MHz) were recorded. The normalized frequency and dissipation shift at the fifth overtone (25 MHz) were used. All the measurements were performed at room temperature. The QCM-D data were modeled using the QTools 3.0 software.

**Preparation of SB-Substituted Chitosans.** Chitosans with various amounts of grafted SB were prepared by reaction of deacetylated chitosan and 3-(dimethyl(2-oxoethyl)ammonio)-propane-1-sulfonate (SB-CHO, see SI-1 for the synthesis and characterization). The method is illustrated here in the case of CH-SB40. A solution of SB-CHO (0.41 g, 2.0 mmol) in methanol (10 mL) was added dropwise to a solution of deacetylated chitosan (0.5 g, 3.1 mmol monosaccharide residues) dissolved in aqueous 20 mL (2 wt %) acetic acid. The reaction was kept at 0 °C and stirred for 30 min. The pH was adjusted to ∼7.0 using 1.0 M aqueous NaOH. The mixture was stirred for 1 h at room temperature. It was cooled back to 0 °C and treated with a solution of sodium cyanoborohydride (0.5 g, 8 mmol) in water (10 mL) added dropwise under stirring. The reaction mixture was stirred overnight at room temperature. It was dialyzed in sequence (membrane of MWCO 6000−8000 kDa) against DI water, aqueous NaOH (0.05 M), aqueous HCl (0.05 M) all for 1 day, and finally against DI water for 2 days. The final product was isolated by lyophilization (yield: 0.53 g). The other SB-substituted chitosans were prepared under identical conditions, except for the initial SB-CHO/$NH_2$ molar ratio (Table 1).

**Preparation of the Polymer Solutions.** Solutions of CH-SB and CH-PC20 were obtained by dissolution of a known amount of polymer in PBS (pH 7.4) to reach a concentration of 1 g $L^{-1}$. Chitosan solutions (1 g $L^{-1}$) were prepared by dissolving CH in a PBS solution containing aqueous acetic acid (2 wt %) followed, after 1 h of stirring at room temperature, by dropwise addition of NaOH to adjust the solution pH to 5. All solutions were kept at room temperature for 12 h prior to measurements.

**Characterization of CH-SB Films by QCM-D.** Gold-coated quartz crystal sensors were cleaned with a piranha solution (concentrated sulfuric acid and hydrogen peroxide (35%) in a 7:3 (v:v) ratio. ***WARNING: Piranha solutions are extremely reactive and must be handled with extreme caution.***), washed with copious amounts of DI water, and dried under nitrogen. The clean sensors were kept overnight in a 1 mM 11-mercaptoundecanoic acid (MUA) solution in ethanol.[18] Subsequently, they were washed with ethanol and dried with nitrogen. The MUA-coated sensors were mounted in the QCM-D flow chamber and flushed with PBS (pH 7.4) until the baseline was stable. A solution of a CH-SB sample in PBS (1 g $L^{-1}$) was introduced in the cell at a flow rate of 20 $\mu$L $min^{-1}$. Once the frequency reached a plateau value, the polymer solution was replaced with PBS to remove the excess polymer. Data were fitted by the Voigt



DOI: 10.1021/acs.langmuir.8b02461
*Langmuir* 2019, 35, 1902−1908

**Table 1. Preparation Conditions and Physicochemical Properties of Zwitterion-Substituted Chitosans**

| polymer[a] | X-CHO/$NH_2$[b] molar ratio | X content (mol %)[c] | $M_w$ (g $mol^{-1}$) | $M_n$ (g $mol^{-1}$) | $M_w/M_n$ |
|---|---|---|---|---|---|
| CH-PC20[d] | 0.2 | 21.8 | $6.3 \times 10^4$ | $4.1 \times 10^4$ | 1.54 |
| CH-SB20 | 0.2 | 22.3 | $5.7 \times 10^4$ | $4.3 \times 10^4$ | 1.33 |
| CH-SB30 | 0.3 | 28.1 | $7.1 \times 10^4$ | $4.9 \times 10^4$ | 1.45 |
| CH-SB40 | 0.4 | 39.7 | $7.3 \times 10^4$ | $4.3 \times 10^4$ | 1.70 |

[a]The molecular weight of the chitosan sample used in all reactions was 50 kDa. [b]Molar percent of X-CHO (X= PC or SB) in the reaction mixture with respect to the molar concentration of the CH glucosamine residues. [c]Average value of the X content in CH-X, determined from the CH-X $^1$H NMR spectra and expressed in molar percent of X-substituted glucosamine residues. [d]Data taken from ref 18.

viscoelastic model, which is widely used for thin polymer films, to calculate the film thickness ($d$).[24,25]

**Interactions of Proteins with CH-SB and CH-PC20 Films.** CH-SB-coated QCM-D sensors, prepared in the QCM-D cell as described above, were treated with a bovine serum albumin (BSA) solution (1 g $L^{-1}$) in PBS introduced at a rate of 20 $\mu$L $min^{-1}$. When the frequency reached a constant value, the QCM-D flow chamber was flushed with PBS to remove the excess unbound protein until the frequency remained stable. For studies of BSA adsorption on CH-PC20, a solution of BSA (1 g $L^{-1}$) in PBS buffer was introduced into the QCM-D cell at a rate of 20 $\mu$L $min^{-1}$, immediately after the preparation of a CH-PC20 film using the protocol described for CH-SB above. Free BSA was removed subsequently by rinsing the chamber with phosphate buffer. All the experiments were performed at 20.00 ± 0.05 °C.

The frequency values obtained after rinsing off the excess protein was used to calculate the amount of protein adsorbed via the Sauerbrey equation[26] (1) often used to determine the surface coverage of thin protein films on QCM-D sensors.[27] The change in frequency ($\Delta f$) is related to the adsorbed protein mass expressed as surface coverage $\Gamma$:

$$\Gamma = -\frac{C\Delta f}{n} \quad (1)$$

$C$ is a constant ($C$ = 0.177 mg $m^{-2}$ $Hz^{-1}$) characteristic of the quartz crystal and $n$ represents the overtone number ($n$ = 1, 3, 5, ...). The change of the dissipation with protein adsorption is correlated to the film viscoelasticity.

**Preparation of Polymer-Coated Substrates for *in Vitro* Assays.** Circular glass coverslips (25 mm in diameter) were placed in ethanol and sonicated for 5 min. They were dried at ambient temperature and exposed to deep-UV irradiation for 10 min. A drop of a solution of CH-SB, CH-PC20, or fibronectin in PBS (0.1 g $L^{-1}$, pH 7.4) or chitosan (0.1 g $L^{-1}$, pH 5) was deposited on a freshly cleaned coverslip. After 1 h, the excess polymer solution was removed by gentle aspiration. The substrate was rinsed with PBS and used immediately

**Cell Culture and Preparation of Cell Aggregates.** WT mouse colon carcinoma CT26 cells (ATCC CRL- 2638; American Tissue Culture Collection) were cultured at 37 °C under a 95% air/5% $CO_2$ atmosphere in a culture medium consisting of Dulbecco's modified eagle medium (DMEM) supplemented with 10% (v/v) fetal bovine serum (FBS) and antibiotics (100 $\mu$g $mL^{-1}$ streptomycin and 100 U $mL^{-1}$ penicillin). Upon reaching confluence, the cells were detached from the flask with trypsin and dispersed in DMEM at a concentration of $4 \times 10^4$ cells $mL^{-1}$. Cellular aggregates were prepared by a modified hanging droplet method.[28] Droplets (15 $\mu$L) of the cell suspension in DMEM were deposited on the inverted lid of a Petri dish. The lid was placed on top of the Petri dish filled with PBS, in order to maintain the droplet under a high humidity atmosphere. Cells fall to the bottom of the droplets due to gravity and adhere to each other. After a 3-day incubation at 37 °C under a 95% air/5% $CO_2$ atmosphere, the aggregates formed in the doplets were deposited on a substrate and used immediately in spreading experiments. In all cases 10 aggregates were monitored under identical conditions.

**Observation of the Spreading of Cellular Aggregates by Bright Field Microscopy.** The polymer-coated coverslips were placed on the bottom of a microscope magnetic observation chamber (Chamlide CMB, CM-B25-1). Droplets containing cellular aggregates were removed from the Petri dish lid with a pipet and placed on the polymer-coated glass coverslips. The microscope cell was filled with $CO_2$-equilibrated culture medium, consisting of DMEM supplemented with 10% (v/v) FBS and antibiotics (100 $\mu$g $mL^{-1}$ streptomycin and 100 U $mL^{-1}$ penicillin) to reach a final volume of 1.5 mL. The chamber was sealed with mineral oil to prevent water evaporation and placed for viewing in an inverted microscope (TIRF AF 6000LX, Leica) equipped with a 10× 0.30 NA objective. Videos were recorded with a CCD camera (Photometrics Cascade 512B, Roper Scientific) at an acquisition rate of 1 frame every 10 min, exported from the instrument software in TIFF format, and visualized

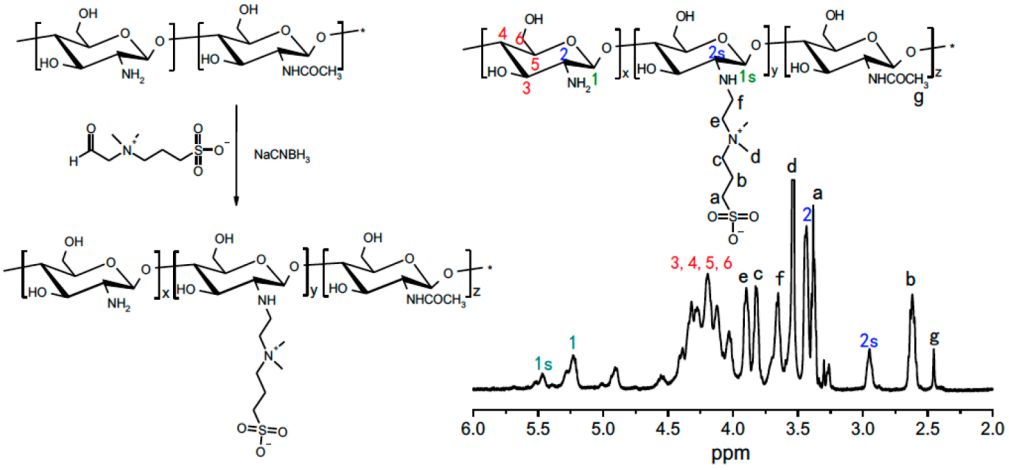


**Figure 1.** $^1$H NMR spectrum of CH-SB40 in $D_2O$/DCl at 70 °C. The SB content was calculated by comparing the integration of the signal at $\delta \sim$ 3.53 ppm (d) due the trimethylammonium protons of the SB residue with that of the signal centered at $\delta$ 4.30 ppm (3, 4, 5, 6) due to the protons 3, 4, 5, 6 of chitosan ($x$ = 58%, $y$ = 40%, and $z$ = 2%).



DOI: 10.1021/acs.langmuir.8b02461
Langmuir 2019, 35, 1902−1908

using the ImageJ software package v.1.46r (National Institutes of Health, Bethesda, MD) at 37 °C.

**Aggregate Spreading Velocity.** The time-dependent area of the precursor film, $A_t$, was determined from bright field micrographs of the aggregates at regular time intervals during the spreading. The contour (perimeter) of the precursor films was traced by hand with ImageJ. The $R_0$ value was determined from $A_0$ (area at time 0) assuming that aggregates are spheres and $A_t$ was determined from the time-dependent micrographs. The slopes of the fitted $A_t/R_0$ lines correspond to the average spreading velocity, $V^* = \pi S/\eta$,of the aggregates, according to eq 2:[29,30]We expect a slowdown of the spreading as S decreases and V* = 0 when S is negative.

$$\frac{A_t}{R_0} = V^* t \tag{2}$$

**Statistical Analysis.** Statistical analysis of the results was performed using a Student *t* test. A *p*-value smaller than or equal to 0.05 was considered as significant.

## RESULTS AND DISCUSSION

**Preparation and Characterization of the CH-SB Samples.** Reductive amination of SB-CHO with primary amine groups of chitosan (Figure 1, left) led to the facile preparation of three CH-SB samples of different levels of SB incorporation (Table 1). The composition of the CH-SB samples was ascertained by $^1$H NMR and FTIR spectroscopy. For instance, in the case of CH-SB40, the $^1$H NMR spectrum (Figure 1) exhibits a singlet at $\delta$ 3.53 ppm (signal d), attributed to the resonance of the trimethylammonium protons ($H_d$) of the sulfobetaine moiety. It also exhibits two distinct signals in the spectral region characteristic of the resonance of the anomeric protons: a signal at $\delta$ 5.19 ppm (signal 1), attributed to the anomeric proton of glucosamine units and a signal at lower field ($\delta$ 5.30 ppm, signal 1s) due to the anomeric proton of the SB-substituted glucosamine units. The resonance of $H_2$ at $\delta$ 3.41 ppm shifts to $\delta$ 2.89 ppm after SB-substitution ($H_{2s}$). Spectra of CH, CH-SB10, CH-SB20, CH-SB30, CH-SB35, and CH-SB40 are presented in Figure SI 1. The IR spectra of CH-SB samples (Figure SI 2) exhibit two bands associated with the sulfobetaine functional group: a band at 1478 cm$^{-1}$, corresponding to the bending of $-N^+(CH_3)_3$ and a band at 728 cm$^{-1}$ due to the S−C stretching mode.[31]

**Physical Properties of the Films and Their Interactions with Proteins.** We used QCM-D to study CH-SB films deposited *in situ* on a mercaptoundecanoic acid MUA/gold-coated quartz crystal following a protocol described previously.[18,32] The changes of the frequency and dissipation recorded for the fifth overtone ($\Delta f_5/5$ and $\Delta D_5/5$), listed in Table 2, were monitored upon formation of CH-SB (Figure SI 3A and B). The thicknesses of the CH-SB films (~20 nm) derived from the Voigt model increase slightly with increasing SB content, as observed also in the case of CH-PC previously reported (film thickness of ~10 nm for CH-PC15 and ~15 nm for CH-PC40).[18] The thin CH-SB and CH-PC20 films prepared here on glass substrates are considered to be rigid surfaces; hence in the following, we will neglect the effect of the film rheology on the adhesion of cells.[33] In a previous study of CH-PC films by takeoff angle-dependent XPS analysis of vacuum-dried CH-PC films, coupled with a QCM-D analysis of the rehydrated films, we established that the vacuum-exposed CH-PC film surface is enriched in PC groups, compared to the film bulk. Moreover, the PC groups remain located preferentially on the water/film interface upon rehydration, due to their hydrophilic nature.[18,36] By analogy, we surmise that during deposition of CH-SB on the substrates, the hydrophilic SB groups preferably orient themselves toward the water/polymer interface rather than being embedded within the polymer.

**Table 2. Properties of CH-SBx and CH-PC20 Films Coated on MUA-Modified Gold Surfaces and Protein Surface Coverage of the Films Obtained from QCM-D Measurements**[a]

| polymer | $\Delta f_5/5$ (Hz) | $\Delta D_5 \times 10^6$ | film thickness (nm) | $\Gamma_{protein}$ ($\mu$g cm$^{-2}$) |
|---|---|---|---|---|
| CH-PC20[b] | −31.8 | 2.8 | 11.8 | 85.9[c] |
| CH-SB20 | −32.3 | 3.4 | 18.7 | 73.5[d] |
| CH-SB30 | −44.8 | 5.2 | 21.4 | 47.1[d] |
| CH-SB40 | −53.8 | 6.1 | 23.6 | 15.5[d] |

[a]$\Delta f_5/5$: frequency shift due to the formation of CH-SB films measured for the 5th overtone. $\Delta D_5$: dissipation change due to the formation of the CH-SB films measured for the 5th overtone. $\Gamma_{protein}$: weight surface coverage of protein on the films. The estimated error in the reported values is 5%. [b]Data taken from ref 17. [c]Fibrinogen surface coverage. [d]BSA surface coverage.

Subsequently, the CH-SB films were treated with a solution of bovine serum albumin (BSA) in PBS. The BSA surface coverages of the three films, estimated by the Sauerbrey equation assuming that the adsorbed BSA formed a single protein layer,[34] are listed in Table 2. Changes of the frequency recorded for the fifth overtone are presented in Figure SI 3C. The BSA coverage decreases significantly as the SB content of the films increases, confirming that the SB substituents endow CH with protein repellency.[35] The protein surface coverage observed for CH-PC20, taken from the previous QCM-D study,[17] is comparable to that recorded of CH-SB20.

**Spreading of CT26 Cell Aggregates on CH-SB, CH-PC20, CH, and Fibronectin Films.** We reported previously that CH and its PC-subsbtituted derivatives adhere strongly on clean hydrophilic glass and readily form a thin film on glass upon dropcasting from a PBS solution and air drying.[18] The CH-SB, CH-PC20, CH, and fibronectin films described here were obtained by the same dropcasting protocol. CT26 cell aggregates (~150 $\mu$m in diameter) prepared by the hanging drop method were placed on polymer-coated coverslips and immersed in cell culture media. Fibronectin and chitosan films are known for their cell-adhesive properties. Accordingly, we observed that CT26 cell aggregates spread on fibronectin and on CH films with formation of a precursor film around them (Figure 2, top rows, where the white lines follow the periphery of the precursor film). Shortly after plating on either fibronectin or CH, elongated isolated cells spread outward from the aggregate forming thin protrusions. At longer times, the escaping cells move collectively. The cell flow is radial and the cells take an elongated form oriented in the direction of the flow. Details of the spreading dynamics are captured in videos presented as SI.

CT26 cell aggregates deposited on CH-PC20 films (Figure 2, row 3 from the top) do not spread as extensively as on CH- and fibronectin-films. Observation of the corresponding video (SI) indicates that, initially, aggregates deposited on CH-PC20 form small protrusions and membrane tubes on their periphery. Single cells progressively emerge from the membrane tubes, adopt an elongated shape, and eventually migrate on the substrate, scouting their surrounding. Cells venturing away from the aggregate often adopt a round shape,



DOI: 10.1021/acs.langmuir.8b02461
Langmuir 2019, 35, 1902−1908

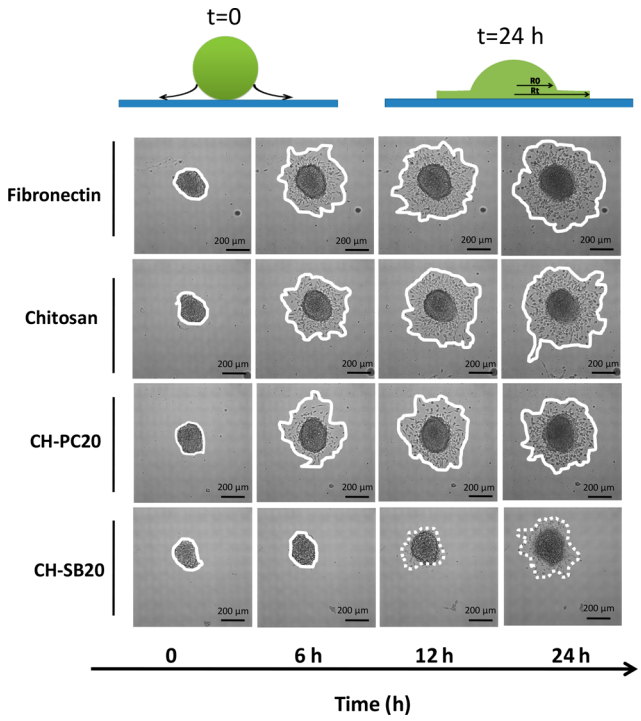


**Figure 2.** Spreading of CT26 cell aggregates over a period of 24 h on fibronectin, chitosan, CH-PC20, and CH-SB20 films coated on glass. The sketches on top of the figure depict slices of an aggregate as deposited on a substrate and after spreading for 24 h on an adhesive substrate (e.g., fibronectin). The white line follows the periphery of the CT26 cell aggregates, including the precursor film, as they expand. The dotted lines in the bottom row indicate the area around the aggregate that encloses all the isolated cells escaped from the aggregate.

an indication that the cell adheres poorly to the film. They move on the substrate in search of adhesive patches onto which they gain an elongated shape. This "schizophrenic" behavior may be attributed to heterogeneities of the film surface not easily detectable by physicochemical measurements. The area of the precursor film is smaller and the film appears less cohesive than in the case of CT26 cell aggregates on CH films.

The escape of cells from CT26 cell aggregates deposited on CH-SB20 films also starts with the formation of protrusions on the aggregate periphery (Figure 2, bottom row and video in SI). Eventually a few rounded cells emerge tethered to the aggregate by membrane tubes. They tug a few neighboring cells while extruding more membrane tubes. Only a few rounded cells escape the aggregate successfully and move freely on their surrounding.

In Figure 3, we present close-up views of CT26 cell aggregates 24 h after deposition on CH-SB40 and CH films, respectively. On CH-SB40 films, the CT26 cell aggregates form an almost spherical cap with a few tethered cells on its periphery. This behavior is close to reaching the limit of partial wetting ($S < 0$).[21] In contrast (Figure 3, left), on CH films CT26 cell aggregates spread with the formation of a precursor film of cells around the aggregate (complete wetting, $S > 0$). Side views of a slice of each aggregates are sketched above the optical micrographs in Figure 3.

The evolution with time of the area of the precursor film, normalized by the initial aggregate radius, is plotted in Figure 4A for CT26 cell aggregates deposited on the polymer films. Since CT26 cell aggregates deposited on CH-SB30 and CH-SB40 films do not form distinct precursor films (see SI Figure 5 and Figure 3 right), we present in an inset on Figure 4A, the changes with time of the normalized area, $A/R_0$. The solid lines in Figure 4 are fits of the data points to a diffusive law. A diffusion coefficient proportional to $R_0$ can be modeled by the following dynamical law for the spread area $A$ versus time $t$: $A(t) = R_0V^*t = Dt$ where $V^* = \pi S/\eta$ is a typical spreading velocity and $R_0$ is the aggregate radius.[37]

The slope of $(A - A_0)/R_0$ or $A/R_0$ fitted lines represents the average spreading velocities, $V^*$, of CT26 cell aggregates, which are presented in Figure 4B. The $V^*$ values are significantly reduced on CH-PC20 and CH-SB20 films, compared to films of unmodified CH. The effect is slightly more pronounced for CH-SB20 vs CH-PC20. Within the CH-

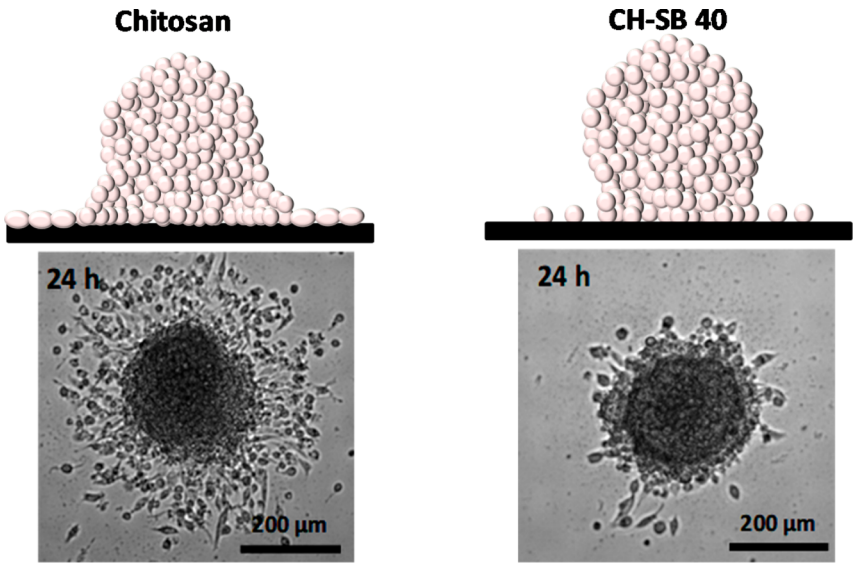


**Figure 3.** Micrograhs of CT26 cell aggregates maintained in cell culture medium for 24 h after deposition on CH (left) and CH-SB40 (right). The sketches above the micrographs represent side views of the aggregates.



DOI: 10.1021/acs.langmuir.8b02461
*Langmuir* 2019, 35, 1902−1908

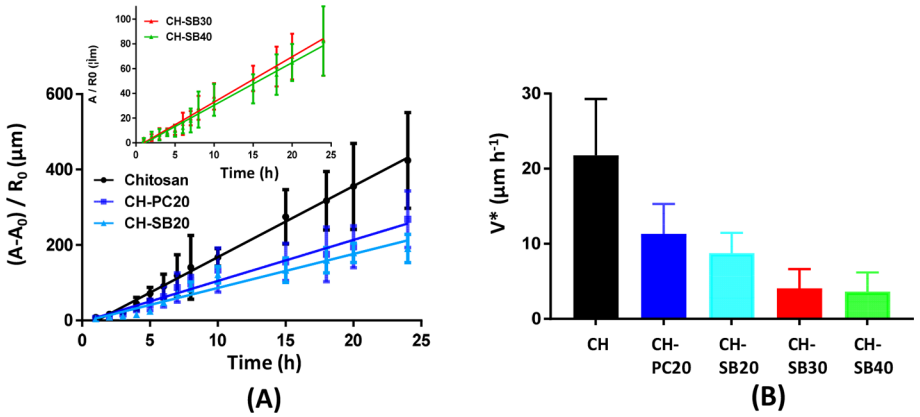


**Figure 4.** (A) Time evolution of the normalized area of the precursor film for CT26 cell aggregates on CH, CH-SB20, and CH-PC20; Inset: Time evolution of the normalized contact area for cell aggregates on CH-SB30 and CH-SB40. (B) Spreading velocity of cell aggregates on various substrates, assuming a diffusional spreading. Data points correspond to the average value of $n$ = 10 aggregates.

SB series, one observes a significant slowdown of the aggregate spreading on CH-SB30 vs CH-SB20. A higher level of SB substitution has no significant effect on $V^*$ (see CH-SB30 vs CH-SB40), which may signal the limit of the sensitivity of CT26 cell aggregates to the adhesivity of CH-SB substrates. In the case of partial wetting, $V^* = 0$, this value is nearly attained for SB30 and SB40 films within the experimental uncertainties (Figure 4B).

## CONCLUSIONS

Sulfobetaine-modified chitosans, as examples of polyzwitterions derived from natural resources, offer several advantages. Their preparation is straightforward, tunable in terms of the level of SB substitution, easily performed under green conditions in standard polymer laboratories, and amenable to scale-up. The preliminary cell aggregate spreading studies on CH-PC20 films suggest that CH-SB surfaces are more effective antifouling substrates than CH-PC films, in agreement with trends reported for other PC/SB substrates. As materials, like chitosan-itself, both CH-SB and CH-PC are biodegradable and adhere strongly to hydrophilic substrates in biological media. We observed on the basis of standard QCM-D measurements, that the films cast from aqueous solutions organize to expose the nonfouling SB or PC units to the water/film interface, a definite advantage in biomedical applications. More generally, we established that the spreading of cell aggregates on nonfouling substrates provides a powerful *in vitro* assay of the nonfouling characteristics. The cancer cell line used here was selected based on its known tendency to form aggregates that are frequently used to test cancer drugs and their formulation *in vitro*. This cell line was useful to report the nonfouling properties of CH-SB, as shown in Figure 3, but was unable to detect differences in adhesivity between CH-SB30 and CH-SB40. By selecting a less cohesive cell line through changes in the cadherin expression level, such as the transfected S180 cell line used in previous studies,[21,22] it may be possible to attain a better sensitivity to subtle changes in nonfouling characteristics.

## ASSOCIATED CONTENT

### Supporting Information

The Supporting Information is available free of charge on the ACS Publications website at DOI: 10.1021/acs.langmuir.8b02461.

Synthesis method and $^1$H NMR spectrum of SB-CHO; the $^1$H NMR and FTIR spectra of deacetylated CH and of all SB-modified chitosans the and IR spectra of CH-SB samples, protein adsorptions; data related to the QCM-D analysis of the formation of CH-SB films and their interaction with BSA and the spreading of CT26 cell aggregates over a period of 24 h on CH-SB30 and CH-SB40 films coated on glass (PDF)

Video of CT26 aggregates spreading onto CH-PC20 (ZIP)

Video of CT26 aggregates spreading onto CH-SB20 (ZIP)

Video of CT26 aggregates spreading onto CH-SB30 (ZIP)

Video of CT26 aggregates spreading onto CH-SB40 (ZIP)

Video of CT26 aggregates spreading onto CH (ZIP)

Video of CT26 aggregates spreading onto fibronectin (ZIP)

## AUTHOR INFORMATION

### Corresponding Author

*E-mail: francoise.winnik@helsinki.fi.

### ORCID

Françoise M. Winnik: 0000-0001-5844-6687

### Notes

The authors declare no competing financial interest.

## ACKNOWLEDGMENTS

We thank Dr. Danijela Vignjevic (UMR 144, Institut Curie, France) for her generous gift of CT26 cells. This study was supported by the NIMS Molecule & Material Synthesis Platform of the "Nanotechnology Platform Project" and the World Premier International Research Center Initiative (WPI), both operated by the Ministry of Education, Culture, Sports, Science and Technology (MEXT), Japan, and by the Natural Sciences and Engineering Research Council of Canada to F.M.W. (Discovery Grant). B.Q. was supported by the National Natural Science Foundation of China (Grant No. 81703457). H.F. was supported by the Special Funds for key innovation team of Zhejiang Province (Grant No. 2010R50017) and Zhejiang Natural Science Foundation (Grant No. LY12B04005).



DOI: 10.1021/acs.langmuir.8b02461
*Langmuir* 2019, 35, 1902−1908

## REFERENCES


(1) Wong, J. Y.; Leach, J. B.; Brown, X. Q. Balance of chemistry, topography, and mechanics at the cell-biomaterial interface: Issues and challenges for assessing the role of substrate mechanics on cell response. *Surf. Sci.* **2004**, *570* (1−2), 119−133.

(2) Chiang, E. N.; Dong, R.; Ober, C. K.; Baird, B. A. Cellular Responses to Patterned Poly(acrylic acid) Brushes. *Langmuir* **2011**, *27* (11), 7016−7023.

(3) Ren, T. C.; Mao, Z. W.; Guo, J.; Gao, C. Y. Directional Migration of Vascular Smooth Muscle Cells Guided by a Molecule Weight Gradient of Poly(2-hydroxyethyl methacrylate) Brushes. *Langmuir* **2013**, *29* (21), 6386−6395.

(4) Ren, X. S.; Wu, Y. Z.; Cheng, Y.; Ma, H. W.; Wei, S. C. Fibronectin and Bone Morphogenetic Protein-2-Decorated Poly-(OEGMA-r-HEMA) Brushes Promote Osseointegration of Titanium Surfaces. *Langmuir* **2011**, *27* (19), 12069−12073.

(5) Wissing, T. B.; Bonito, V.; Bouten, C. V. C.; Smits, A. Biomaterial-driven in situ cardiovascular tissue engineering-a multi-disciplinary perspective. *npj Regen. Med.* **2017**, *2*, 20.

(6) Pape, A. C. H.; Ippel, B. D.; Dankers, P. Y. W. Cell and Protein Fouling Properties of Polymeric Mixtures Containing Supramolecular Poly(ethylene glycol) Additives. *Langmuir* **2017**, *33* (16), 4076−4082.

(7) Andruzzi, L.; Senaratne, W.; Hexemer, A.; Sheets, E. D.; Ilic, B.; Kramer, E. J.; Baird, B.; Ober, C. K. Oligo(ethylene glycol) containing polymer brushes as bioselective surfaces. *Langmuir* **2005**, *21* (6), 2495−2504.

(8) Schlenoff, J. B. Zwitteration: Coating Surfaces with Zwitterionic Functionality to Reduce Nonspecific Adsorption. *Langmuir* **2014**, *30* (32), 9625−9636.

(9) Jiang, S. Y.; Cao, Z. Q. Ultralow-Fouling, Functionalizable, and Hydrolyzable Zwitterionic Materials and Their Derivatives for Biological Applications. *Adv. Mater.* **2010**, *22* (9), 920−932.

(10) Chen, S. F.; Li, L. Y.; Zhao, C.; Zheng, J. Surface hydration: Principles and applications toward low-fouling/nonfouling biomaterials. *Polymer* **2010**, *51* (23), 5283−5293.

(11) Leng, C.; Hung, H. C.; Sieggreen, O. A.; Li, Y. T.; Jiang, S. Y.; Chen, Z. Probing the Surface Hydration of Nonfouling Zwitterionic and Poly(ethylene glycol) Materials with Isotopic Dilution Spectroscopy. *J. Phys. Chem. C* **2015**, *119* (16), 8775−8780.

(12) Leng, C.; Han, X. F.; Shao, Q.; Zhu, Y. H.; Li, Y. T.; Jiang, S. Y.; Chen, Z. In Situ Probing of the Surface Hydration of Zwitterionic Polymer Brushes: Structural and Environmental Effects. *J. Phys. Chem. C* **2014**, *118* (29), 15840−15845.

(13) Feng, W.; Zhu, S. P.; Ishihara, K.; Brash, J. L. Adsorption of fibrinogen and lysozyme on silicon grafted with poly(2-methacryloyloxyethyl phosphorylcholine) via surface-initiated atom transfer radical polymerization. *Langmuir* **2005**, *21* (13), 5980−5987.

(14) Yang, W.; Chen, S. F.; Cheng, G.; Vaisocherova, H.; Xue, H.; Li, W.; Zhang, J. L.; Jiang, S. Y. Film thickness dependence of protein adsorption from blood serum and plasma onto poly(sulfobetaine)-grafted surfaces. *Langmuir* **2008**, *24* (17), 9211−9214.

(15) Cheng, G.; Li, G. Z.; Xue, H.; Chen, S. F.; Bryers, J. D.; Jiang, S. Y. Zwitterionic carboxybetaine polymer surfaces and their resistance to long-term biofilm formation. *Biomaterials* **2009**, *30* (28), 5234−5240.

(16) Du, Y.; Gao, J. Y.; Chen, T. T.; Zhang, C.; Ji, J.; Xu, Z. K. Understanding the Oxidative Stability of Antifouling Polymer Brushes. *Langmuir* **2017**, *33* (29), 7298−7304.

(17) Tiera, M. J.; Qiu, X. P.; Bechaouch, S.; Shi, Q.; Fernandes, J. C.; Winnik, F. M. Synthesis and characterization of phosphorylcholine-substituted chitosans soluble in physiological pH conditions. *Biomacromolecules* **2006**, *7* (11), 3151−3156.

(18) Qi, B. W.; Kujawa, P.; Toita, S.; Beaune, G.; Winnik, F. M. Phosphorylcholine-Modified Chitosan Films as Effective Promoters of Cell Aggregation: Correlation Between the Films Properties and Cellular Response. *Macromol. Biosci.* **2015**, *15* (4), 490−500.

(19) Zhang, Z.; Chen, S. F.; Chang, Y.; Jiang, S. Y. Surface grafted sulfobetaine polymers via atom transfer radical polymerization as superlow fouling coatings. *J. Phys. Chem. B* **2006**, *110* (22), 10799−10804.

(20) Steinberg, M. S. Reconstruction of Tissues by Dissociated Cells. *Science* **1963**, *141* (3579), 401−408.

(21) Douezan, S.; Brochard-Wyart, F. Dewetting of cellular monolayers. *Eur. Phys. J. E: Soft Matter Biol. Phys.* **2012**, DOI: 10.1140/epje/i2012-12034-9.

(22) Beaune, G.; Duclos, G.; Khalifat, N.; Stirbat, T. V.; Vignjevic, D. M.; Brochard-Wyart, F. Reentrant wetting transition in the spreading of cellular aggregates. *Soft Matter* **2017**, *13* (45), 8474−8482.

(23) Ishiguro, T.; Ohata, H.; Sato, A.; Yamawaki, K.; Enomoto, T.; Okamoto, K. Tumor-derived spheroids: Relevance to cancer stem cells and clinical applications. *Cancer Science* **2017**, *108* (3), 283−289.

(24) White, C. C.; Schrag, J. L. Theoretical predictions for the mechanical response of a model quartz crystal microbalance to two viscoelastic media: A thin sample layer and surrounding bath medium. *J. Chem. Phys.* **1999**, *111* (24), 11192−11206.

(25) Voinova, M. V.; Rodahl, M.; Jonson, M.; Kasemo, B. Viscoelastic acoustic response of layered polymer films at fluid-solid interfaces: Continuum mechanics approach. *Phys. Scr.* **1999**, *59* (5), 391−396.

(26) Kankare, J. Sauerbrey equation of quartz crystal microbalance in liquid medium. *Langmuir* **2002**, *18* (18), 7092−7094.

(27) Voros, J. The density and refractive index of adsorbing protein layers. *Biophys. J.* **2004**, *87* (1), 553−561.

(28) Marmottant, P.; Mgharbel, A.; Kafer, J.; Audren, B.; Rieu, J. P.; Vial, J. C.; van der Sanden, B.; Maree, A. F. M.; Graner, F.; Delanoe-Ayari, H. The role of fluctuations and stress on the effective viscosity of cell aggregates. *Proc. Natl. Acad. Sci. U. S. A.* **2009**, *106*, 17271.

(29) Saez, A.; Anon, E.; Ghibaudo, M.; du Roure, O.; Di Meglio, J. M.; Hersen, P.; Silberzan, P.; Buguin, A.; Ladoux, B. Traction forces exerted by epithelial cell sheets. *J. Phys.: Condens. Matter* **2010**, *22* (19), 194119.

(30) Trepat, X.; Wasserman, M. R.; Angelini, T. E.; Millet, E.; Weitz, D. A.; Butler, J. P.; Fredberg, J. J. Physical forces during collective cell migration. *Nat. Phys.* **2009**, *5* (6), 426−430.

(31) Bu, L. T.; Straub, J. E. Vibrational frequency shifts and relaxation rates for a selected vibrational mode in cytochrome c. *Biophys. J.* **2003**, *85* (3), 1429−1439.

(32) Qi, B.; Shimizu, Y.; Nakanishi, J.; Winnik, F. M. Estradiol-tethered micropatterned surfaces for the study of estrogenic non-genomic pathways. *Chem. Commun.* **2016**, *52* (65), 10056−10059.

(33) Gupta, M.; Sarangi, B. R.; Deschamps, J.; Nematbakhsh, Y.; Callan-Jones, A.; Margadant, F.; Mege, R. M.; Lim, C. T.; Voituriez, R.; Ladoux, B. Adaptive rheology and ordering of cell cytoskeleton govern matrix rigidity sensing. *Nat. Commun.* **2015**, DOI: 10.1038/ncomms8525.

(34) Phan, H. T. M.; Bartelt-Hunt, S.; Rodenhausen, K. B.; Schubert, M.; Bartz, J. C. Investigation of Bovine Serum Albumin (BSA) Attachment onto Self-Assembled Monolayers (SAMs) Using Combinatorial Quartz Crystal Microbalance with Dissipation (QCM-D) and Spectroscopic Ellipsometry (SE). *PLoS One* **2015**, *10* (10), e0141282.

(35) Schmidt, S.; Madaboosi, N.; Uhlig, K.; Kohler, D.; Skirtach, A.; Duschl, C.; Mohwald, H.; Volodkin, D. V. Control of Cell Adhesion by Mechanical Reinforcement of Soft Polyelectrolyte Films with Nanoparticles. *Langmuir* **2012**, *28* (18), 7249−7257.

(36) Miao, Z. M.; Kujawa, P.; Lau, Y. T. R.; Toita, S.; Qi, B. W.; Nakanishi, J.; Cloutier, I.; Tanguay, J. F.; Winnik, F. M. Tuning the Properties and Functions of 17 beta-Estradiol-polysaccharide Conjugates in Thin Films: Impact of Sample History. *Biomacromolecules* **2012**, *13* (12), 4098−4108.

(37) Beaune, G.; Stirbat, T. V.; Khalifat, N.; Cochet-Escartin, O.; Garcia, S.; Gurchenkov, V. V.; Murrell, M. P.; Dufour, S.; Cuvelier, D.; Brochard-Wyart, F. How cells flow in the spreading of cellular aggregates. *Proc. Natl. Acad. Sci. U. S. A.* **2014**, *111* (22), 8055−8060.




DOI: 10.1021/acs.langmuir.8b02461
*Langmuir* 2019, 35, 1902−1908